2.6 FRICTION STIR WELDING OF ODS STEELS AND ADVANCED FERRITIC STRUCTURAL STEELS

- Z. Feng, W. Tang, X. Yu, G. Chen, D. Hoelzer, and L. Tan (Oak Ridge National Laboratory)

OBJECTIVE

This project addresses the critical technology gap of joining oxide dispersion strengthened (ODS) steels, nanostructured ferritic alloys (NFAs), reduced-activation ferritic/martensitic (RAFM) steels, and dissimilar metal joining of ODS/NFAs and RAFM steels through friction stir welding technology. The research focuses on understanding the stability of the strengthening phases in the weld region, and the bonding mechanisms between dissimilar structural steels as a function of FSW process conditions.

Specific project objectives are (i) developing the process parameter space to consistently produce defect-free welds of the same and dissimilar metals, (ii) developing the knowledge base and practical applicable approaches to tailor and optimize the microstructure features in the weld to match the properties of the base metal through process innovation, and (iii) producing representative weld joints and welded components to support future testing and evaluation at high temperature and irradiation environments in collaboration with JAEA and other international teams.

SUMMARY

Research during this period focused on (1) designing and developing a FSW process to join 14YWT ODS steel and an ORNL developed 9Cr steel, referred as modified 9Cr steel in this report, (2) dissimilar materials FSW microstructure characterization and flow pattern interpretation, (3) understanding the effect of FSW process conditions on the nano oxide strengthening particles in 14YWT ODS alloy, and (4) CFD based computer modeling to predict temperature fields and reveal flow fields in FSW. We successfully joined 14YWT ODS alloy and modified 9Cr steel without any defects, found FSW temperatures could be high enough to cause the modified 9Cr quenching in the stir zone. The thermal – mechanical process in FSW resulted in nanoparticle coarsening but the process could be finely tuned to preserve nanoclusters with slight coarsening on the 14YWT side of the stir zone. Computer modeling further revealed FSW thermal – mechanical mechanisms.

PROGRESS AND STATUS

Dissimilar materials ODS alloy and RAFM steel FSW and characterization

Previously, the project team has successfully made various friction stir welds on OSD and RAMF advanced steels, including dissimilar welds between ODS and RAMF. These welds were extensively characterized [1-6]. In this period, a defect free dissimilar material FSW butt joint of 14YWT and the modified 9Cr steel was made with the weld center line skewed with the material interface at 9.6°, see Figure 1 for the welded joint. Three metallographic specimens were cut from the weld at locations shown in Figure 1. Section (A), where the interface between ODS and RAFM steel began to intercept the periphery of the pin and experience the stirring effect of the pin; Section (B), where the interface was coincident with the pin axis, and Section (C), where the pin began to leave the interface. All three specimens were ground, polished and etched with 5 ml HNO3 + 1 ml HF + 50 ml distilled water etchant. Material microstructures at various metallurgical zones were observed under an optical microscope and Vickers hardness mapping test was applied on the joint cross section. All three joint cross sections with the scaled FSW tool shoulder diameter and pin shape are shown in Figure 2.

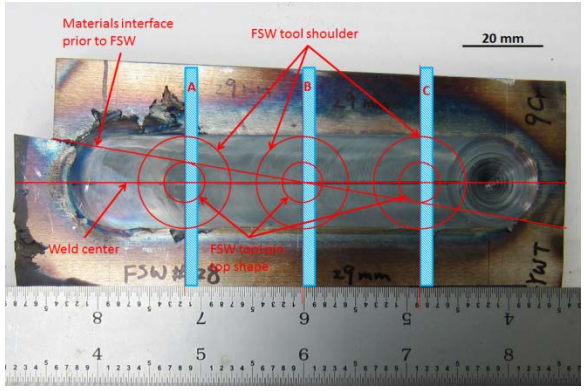

Figure 1. Dissimilar materials 14YWT ODS alloy & modified 9Cr steel FSW joint

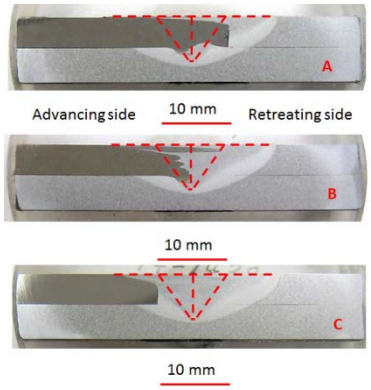

Figure 2. 14YWT ODS alloy & modified 9Cr steel FSW joint cross sections at various locations

As shown in Figure 2, materials mainly stayed at their own sides under the actions of the rotating tool, but some mixing in both horizontal and vertical directions is observed. It is clear that this material mixing neither random nor total mixing, but like a laminar overlap with a specific pattern, i.e., materials close to the top surface flowed and mixed more on the horizontal plane affected by the tool shoulder motion, while materials away from the top surface flowed and mixed both in vertical and horizontal planes influenced by the tool pin. Detailed flow patterns are shown in Figure 3 for Section B, where 14YWT is represented by dark color in the scanned cross section but by white color in microstructure pictures. In Figure 3, the modified 9Cr steel, which was located on the retreating side of the joint, flowed up and towards the advancing side, while 14YWT, which was located on the advancing side of the joint, flowed down and towards the retreating side. As a result, the first layer material at the top of the stir zone under the shoulder influence is always the modified 9Cr steel.

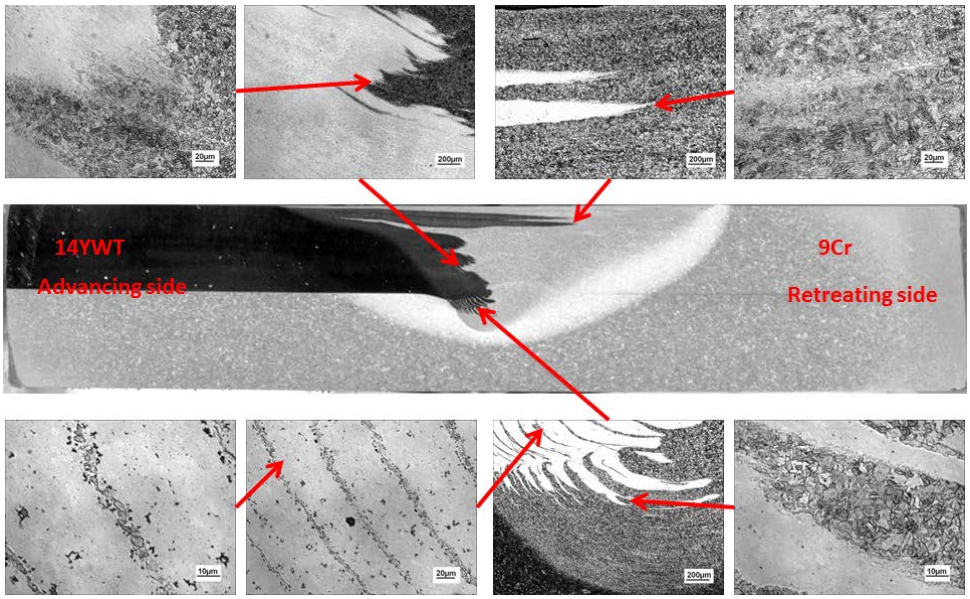

Figure 3. Materials flow pattern in dissimilar materials 14YWT – modified 9Cr FSW joint

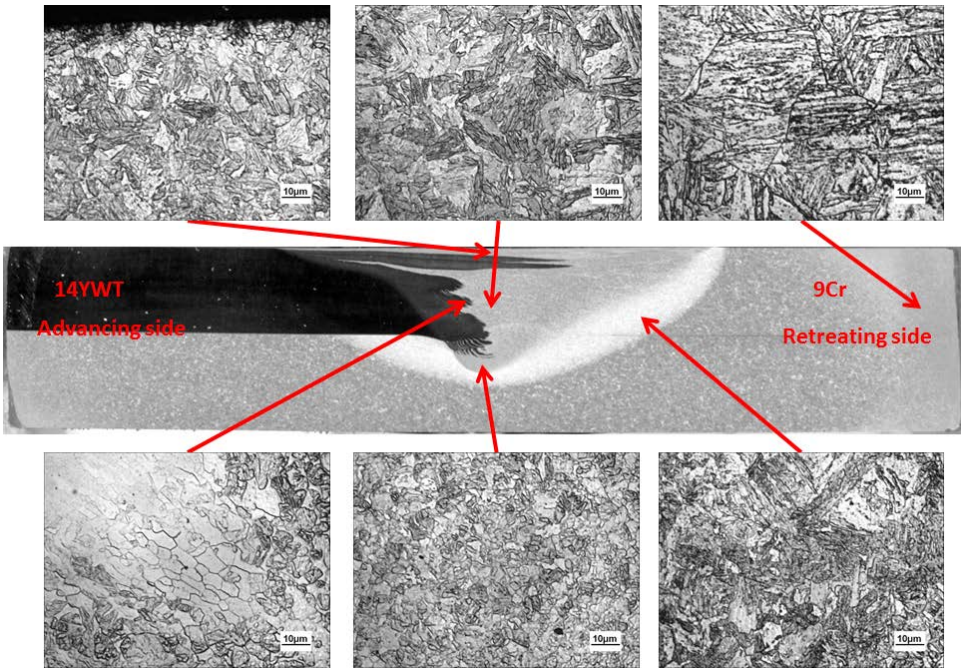

Figure 4. Microstructure of dissimilar materials 14YWT – modified 9Cr FSW joint

Optical microscope observation showed the FSW joint is free from defects for specimen B, where the original interface is aligned with the welding centerline, and microstructures in various metallurgical zones are shown in Figure 4. For base metals, a martensitic microstructure was observed with modified 9Cr steel but 14YWT grain structure can't be recognized under optical microscope due to its submicron size. In the stir zone, modified 9Cr remains martensitic and grain size at the bottom is obvious smaller than that in the middle or at the top due to the FSW temperature distributions. 14YWT grains are observed in the stir zone because they have enlarged from submicron to micron size due to the FSW heat input. In

addition, 14YWT grains do not present as equiaxed shape, but their major axis is along the material flow direction.

Vickers microhardness mapping was used on the dissimilar materials FSW cross sections to investigate the FSW thermal – mechanical effects on both materials' mechanical properties, as well as to estimate the FSW temperature range since it is hard, if not impossible, to precisely measure stir zone temperature during FSW. Micro-hardness mapping and the corresponding cross section specimen are shown in Figure 5. From Figure 5, ODS material 14YWT, which is located on the upper left side, softened in the stir zone while modified 9Cr steel hardened in the stir zone. This matches the microstructure observations in Figure 4 of 14YWT grain growth and martensitic modified 9Cr in the stir zone. Furthermore, the current FSW temperature must have exceeded the modified 9Cr phase transformation temperature and could have affected nanoparticles in ODS material 14YWT.

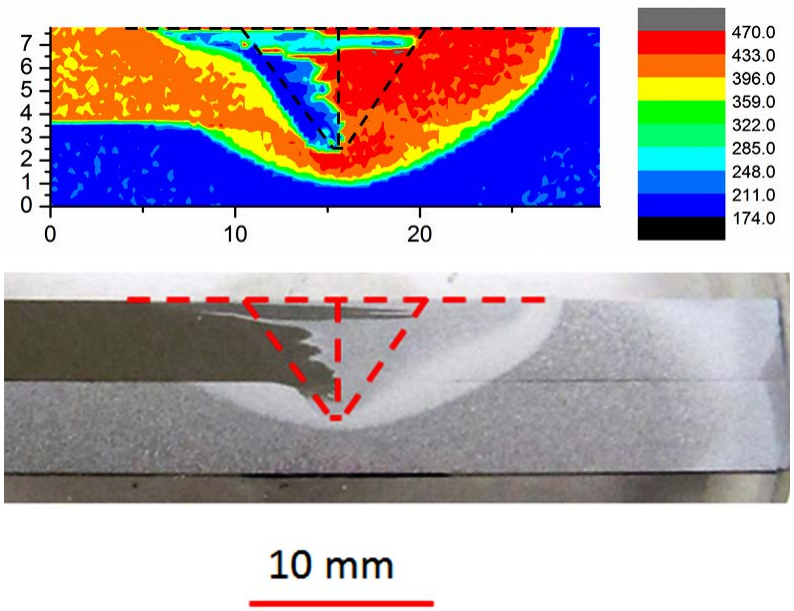

Figure 5. 14YWT & modified 9Cr FSW joint cross section and microhardness mapping

Atom probe tomography (APT) of 14YWT ODS alloy FSW

Atom probe tomography (APT) and electron backscatter diffraction (EBSD) analyses have been used on a 14YWT ODS steel/F82H steel FSW lap joint, mainly focused on the ODS material 14YWT. The APT measurements were carried out with datasets between 100 and >500 million atom collected for each condition, so that the overall distribution of nanocluster precipitates could be evaluated. Major findings are presented in Figures 6 to 9. Firstly, the average size of the grains in the stir zone was estimated to be 1.8 ± 0.4 μm compared with 1.1 ± 0.6 μm in the base metal. The mean radius of the nanoclusters increased from 1.9 ± 0.6 nm in the base condition to 2.7 ± 1.4 nm and 2.9 ± 1.4 nm, respectively in the stir and mixing zones. Secondly, the size increase is also reflected in the range of nanocluster precipitates sizes observed, i.e., the maximum precipitate increased from 4.3 nm in the base material to 18.0 and 11.0 nm, respectively in the stir and mixing zones, as well as the increases in the skewness and Kurtosis parameters. The average number densities of the nanocluster were estimated to be 5.2×10^{22}, 2.3×10^{22}, and 6.4×10^{22} m^{-3}, for the base metal, stir zone, and mixing zone, respectively. However, variations from 1.4×10^{21} m^{-3} to 5.2×10^{22} m^{-3} in the base metal (with an average of 1.4×10^{22} m^{-3}) and between 2.3×10^{22} and 7.1×10^{22} m^{-3} (with an average of 4.3×10^{22} m^{-3}) in the stir zone were observed in other datasets. These averaged are based on 144, 2072, and 696 precipitates, respectively for the base metal, stir zone and mixing zone, and a total of 2.5 billion atoms. Finally, post weld heat treatment didn't affect nanoclusters characteristics in the FSW joint.

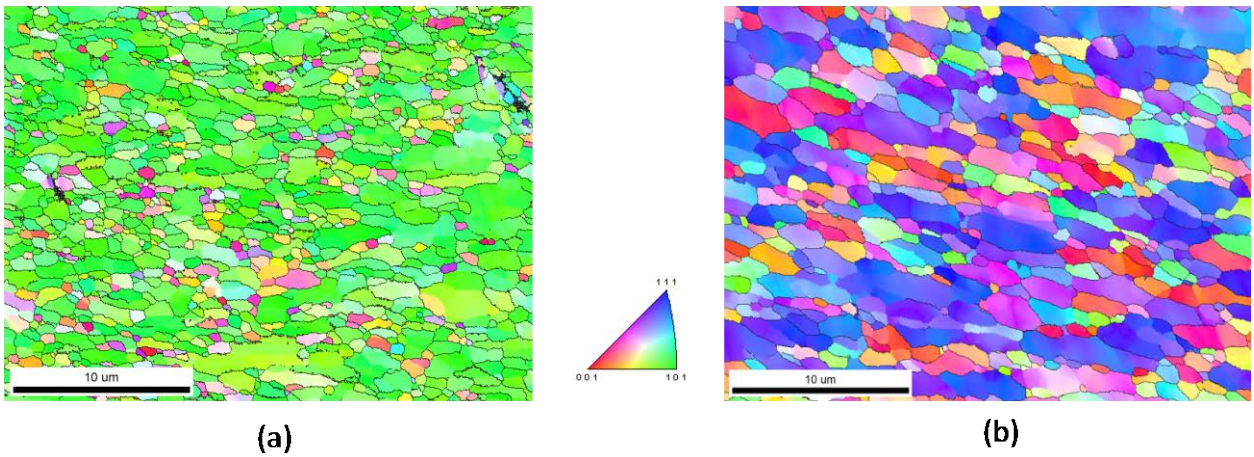

Figure 6. EBSD maps of (a) base metal (b) stir zone.

in nm	Base metal	Stir zone	TMAZ
Mean	1.91	2.69	2.94
Mode	1.56	1.63	1.58
Median	1.76	2.38	2.63
Minimum	0.90	0.71	0.92
Maximum	4.29	18.02	11.01
Skewness	1.18	3.26	1.87
Kurtosis	1.35	24.00	5.38

(a) As welded

in nm	Base metal	Stir zone	TMAZ zone (B)
Mean	1.6	2.0	2.3
Mode	1.0	0.83	1.94
Median	1.4	1.8	1.94
Minimum	0.5	0.55	0.52
Maximum	4.36	7.5	10.4
Skewness	1.07	1.42	1.85
Kurtosis	0.86	3.95	5.68

(b) Post weld heat treated

Figure 7. Nanoparticles atom probe characterization of ODS 14YWT base metal and FSW

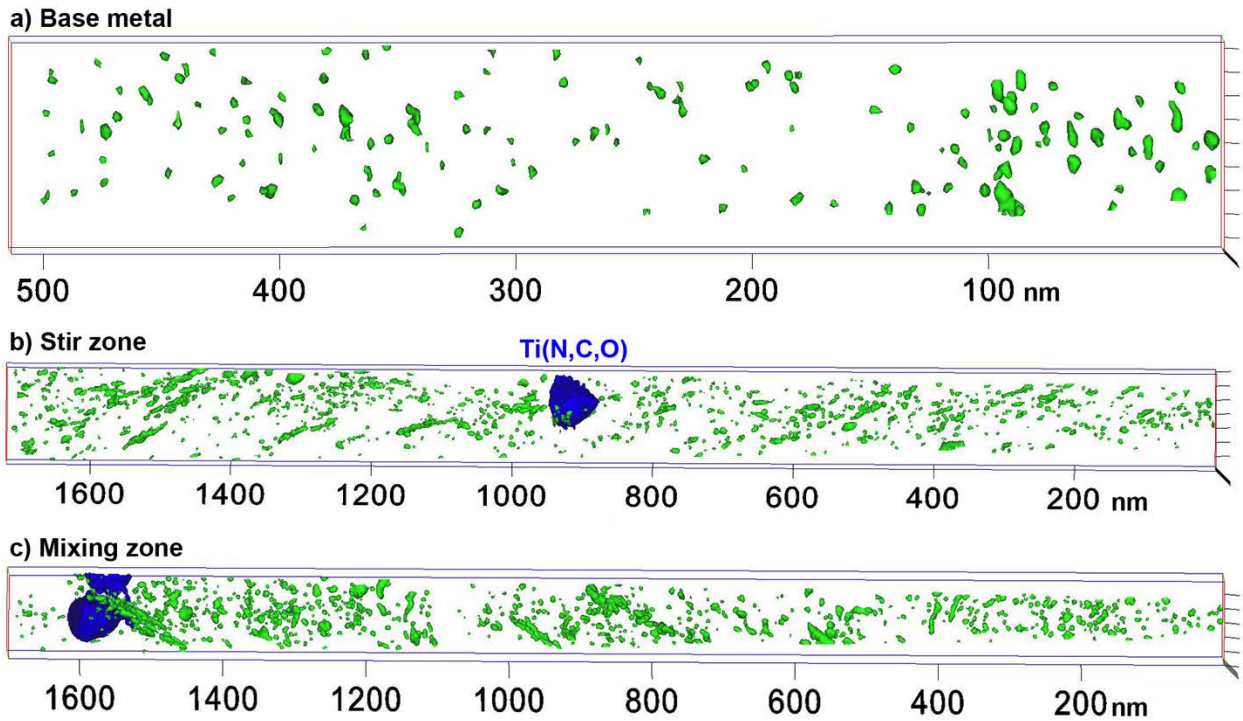

Figure 8. 5 at.% Ti isoconcentration surfaces of base metal, stir zone and mixing zone.

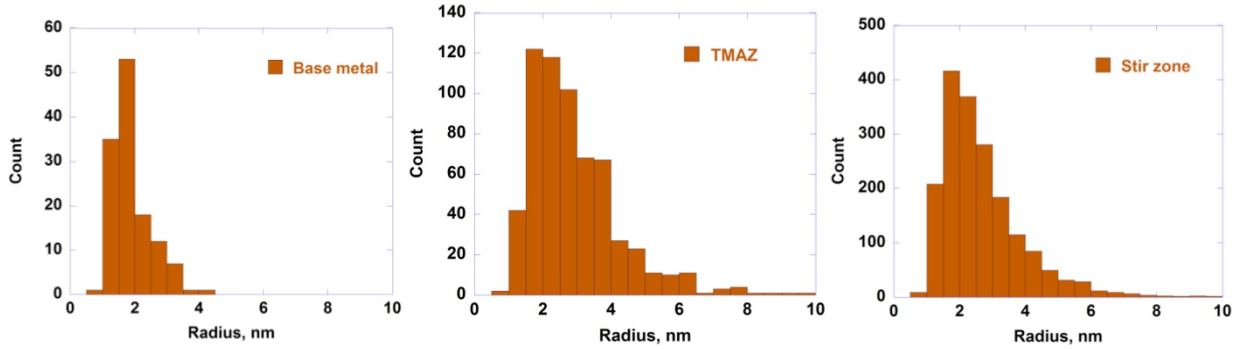

Figure 9. histograms of precipitates distribution in the base metal, TMAZ and stir zone.

Overall, the friction stir welding resulted in insignificant increase in average grain size and the radius of nanocluster precipitates, for the 14YWT/F82H lap joint FSW process conditions. Further investigation of the dissimilar materials FSW shown in Figure 1 will be carried out to reveal heat input effects on nanoparticles dimensions; however, consider the hardness drop of the ODS alloy after FSW shown in Figure 5, low heat input FSW is one of the keys to join ODS material without changing grain sizes and nanoparticle dimensions.

Friction-induced material behavior in FSW thermal-mechanical coupled computer modeling

The two fundamental key points regarding the thermal-mechanical conditions experienced by FSW are temperature and material deformation, which affect joints metallographic characterization and properties. However, it is extremely difficult or impossible to determine the thermal-mechanical fields accurately in FSW because they are coupled dynamic processes surrounded by solid metals. On the other hand, computational modeling, when appropriately constructed and performed, can simulate the complicated

processes and provide insights into the temperature and deformation during FSW, to guide FSW process development and optimization. To study the fundamental variables of FSW in joining ODS and RAFM steels, such as temperature, strain, strain rate and flow stress, 3D thermally and mechanically coupled numerical models were developed based on Computational Fluid Dynamics (CFD). In the model presented here, basic variables describing the heat flow and material flow in FSW are temperature and material velocity, which are obtained by solving governing equations in Eulerian formulation. The conservation equations of mass and momentum for incompressible single-phase flow are given by,

$$\nabla \cdot (\rho \vec{v}) = 0 \tag{1}$$

$$\nabla \cdot (\rho \vec{v}\vec{v}) = -\nabla p + \nabla \cdot \left(\mu(\nabla \vec{v} + \nabla \vec{v}^T)\right) \tag{2}$$

Where ρ is the density, μ is the viscosity, p is the pressure and $\vec{v}$ is the fluid velocity.

The energy conservation equation is given by,

$$\nabla \cdot (\vec{v}H) = \nabla \cdot (k\nabla T + S_V) \tag{3}$$

Where H is the enthalpy, T is the temperature, k is the thermal conductivity and S_V is a spatial source term regarding the heat generation due to plastic deformation.

Two tool pin configurations are chosen in the current modeling, with step spiral and without step spiral, which are shown in Figure 10.

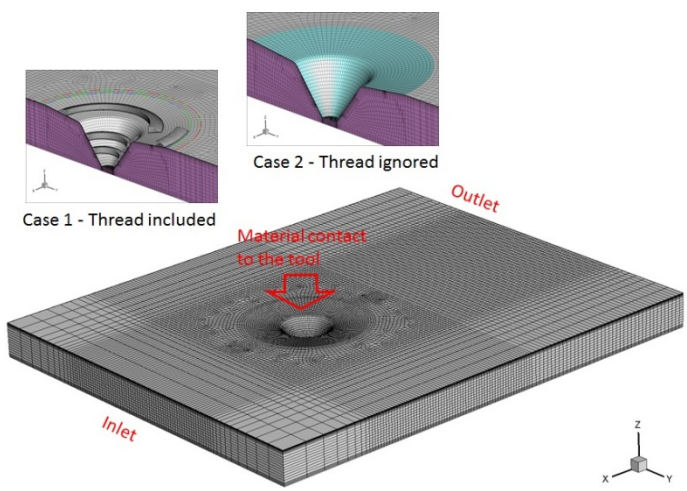

Figure 10. FSW process CFD computer model

A typical temperature field from FSW modeling is shown in Figure 11. From Figure 11, it is found that the predicted temperature field matches a typical FSW temperature distribution, where a localized high temperature area exists in the vicinity of the FSW tool and the temperature gradient is steeper in front of the tool than at back of the tool. The predicted peak temperature, 1326°C, was located close to the shoulder. This predicted stir zone temperature, which is higher than the modified 9Cr steel phase transformation temperature and 14YWT base metal heat treatment temperature, quenched the modified 9Cr and enlarged 14YWT grain sizes in the stir zone, and resulted in modified 9Cr hardening as well as 14YWT softening in the same metallurgical zone. Moreover, the step spiral pin tool caused more material deformation and resulted in higher welding temperature in FSW than the smooth pin tool, see Figure 12.

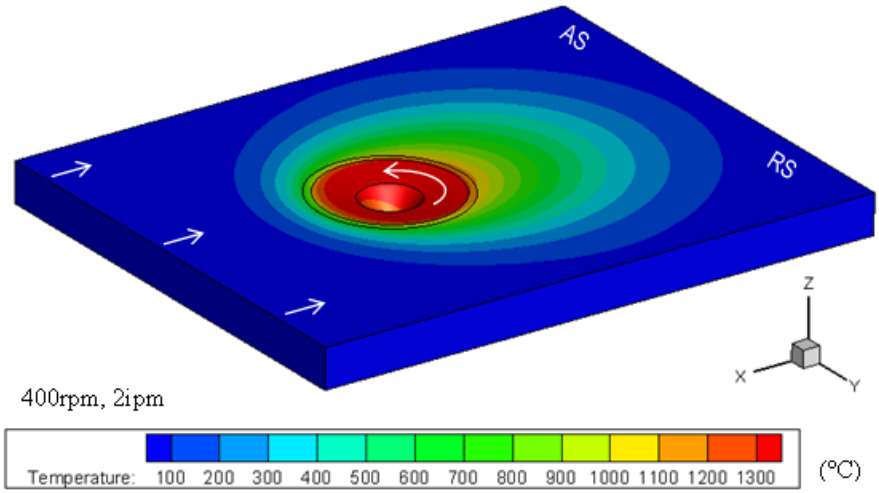

Figure 11. FSW temperature field from computer modeling

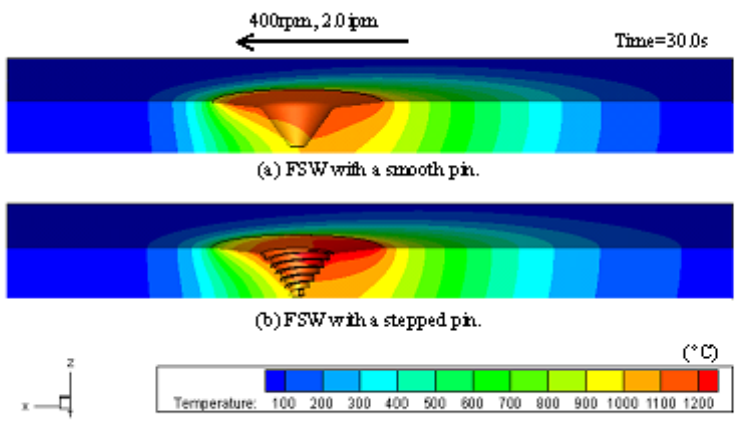

Figure 12. FSW Temperature fields established with and without pin step spirals

Material flow patterns are visualized by flow paths as shown in Figure 13. In order to capture the influence of tool on material flow, marker materials were released at different heights through the workpiece thickness, i.e., 1 mm (Figure 13(a)), 3 mm (Figure 13(b)), and 6 mm (Figure 13(c)) underneath the workpiece and tool shoulder interface, respectively. From Figure 13(a), it is clear that material on the advancing side flows up and towards the retreating side, while material on the retreating side flows down and towards the advancing side. Similar patterns show in Figure 13(b) but with less mixing, and Figure 13(c) showed the least deviation from their original flow path. Overall, flow paths predicted by the computer modeling in Figure 13 matches the FSW joint cross section materials flow pattern observations in Figure 3 and Figure 4, i.e., the modified 9Cr, which was located on the retreating side of the joint, rotated with the tool and moved up towards the plate top, while 14YWT, which was located on the advancing side of the joint, rotated and moved down to the plate bottom.

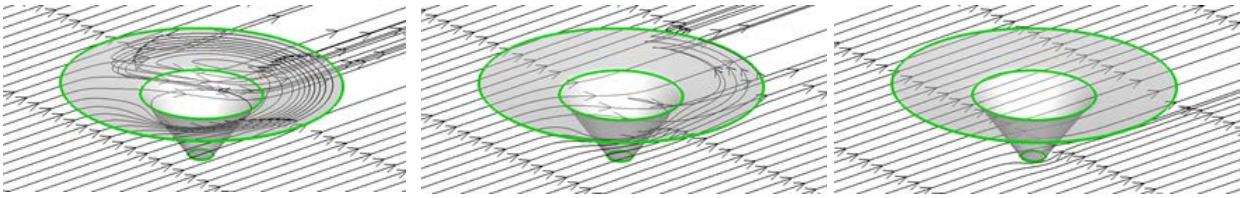

(a) 1 mm underneath shoulder (b) 3 mm underneath shoulder (c) 6 mm underneath shoulder

Figure 13. Flow pattern predictions by CFD computer modeling (Advancing side on the right and retreating side on the left)

FSW flow fields from the modeling indicate that step spiral pin tool caused more flow and a wider flow zone than smooth pin tool, see Figure 14 for details. Moreover, heavier flow close to the tool shoulder shown in Figure 14 explains more changes on microstructure characterization and microhardness distribution at the same region than areas close to the plate bottom from the experimental results.

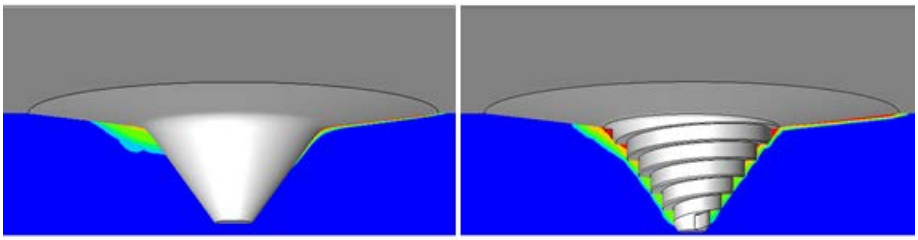

(a) Smooth pin (b) Step Spiral pin

Figure 14. FSW flow fields established with and without pin step spirals

Future Work

The following major activities are planned for the next 6 months:

- Produce additional RAFM steel FSW joints for high temperature creep tests.
- Preparing necessary plans and schedules for high temperature creep test with in-situ local deformation measurement to reveal high temperature creep resistance capabilities of materials at various metallurgical zones in a FSW joint.
- Further APT characterization of nano particles/clusters in the dissimilar FSW of 14YWT ODS alloy and the modified 9Cr steel to further understand FSW heat input effects to nanoclusters and ODS materials properties.
- Further computer modeling to reveal point by point thermal – mechanical history in FSW process for further understanding FSW fundamentals.

References

[1] D.T. Hoelzer, K.A. Unocic, M.A. Sokolov, and Z. Feng, "Joining of 14ywt and F82h by Friction Stir Welding," J. Nucl. Mater., 442 (1–3, Supplement 1) (2013) S529-S534.

[2] Z. Yu, Z. Feng, D.T. Hoelzer, L. Tan, M.A. Sokolov, “Friction Stir Welding of ODS Steels and Advanced Ferritic Structural Steels,” ICFRM16, Oct 20-26, 2013, Beijing, China.

[3] D.T. Hoelzer, K.A. Unocic, M.A. Sokolov, and Z. Feng, "Joining of 14ywt and F82h by Friction Stir Welding," ICFRM-15 15th (International Conference on Fusion Reactor Materials), 442, (2013), S529-S534.

[4] Z. Yu, Z. Feng, D.T. Hoelzer, L. Tan, M.A. Sokolov, “Similar and Dissimilar Friction Stir Welding of ODS and RAFM Steels,” TMS Annual Meeting, Feb 16-20, 2014, San Diego, CA.

[5] X. Chen, Z. Yu, and Z. Feng, “FSW of Reduced Activations Steels with PWHT,” 10th International Friction Stir Welding Symposium, May 20-22, 2014, Beijing, China.
[6] X. Yu, B. Mazumder, M. K. Miller, S. A. David, and Z. Feng, “Stability of Y–Ti–O Precipitates in Friction Stir Welded Nanostructured Ferritic Alloys”, Science and Technology of Welding and Joining, Accepted.